

This is the accepted manuscript made available via CHORUS. The article has been published as:

# Benchmarking the pseudopotential and fixed-node approximations in diffusion Monte Carlo calculations of molecules and solids

R. Nazarov, L. Shulenburger, M. Morales, and Randolph Q. Hood

Phys. Rev. B **93**, 094111 — Published 28 March 2016

DOI: [10.1103/PhysRevB.93.094111](https://doi.org/10.1103/PhysRevB.93.094111)

# Benchmarking the pseudopotential and fixed-node approximations in diffusion Monte Carlo calculations of molecules and solids

R. Nazarov<sup>a</sup>, L. Shulenburger<sup>b</sup>, M. Morales<sup>a</sup> and Randolph Q. Hood<sup>a</sup>

<sup>a</sup>Lawrence Livermore National Laboratory, Livermore, California 94550, USA

<sup>b</sup>Sandia National Laboratories, Albuquerque, New Mexico 87185, USA

## Abstract

We performed diffusion Monte Carlo (DMC) calculations of the spectroscopic properties of a large set of molecules assessing the effect of different approximations. In systems containing elements with large atomic numbers we show that the errors associated with the use of nonlocal mean-field based pseudopotentials in DMC calculations can be significant and may surpass the fixed-node error. We suggest practical guidelines for reducing these pseudopotential errors, which allow us to obtain DMC-computed spectroscopic parameters of molecules and equation of state properties of solids in excellent agreement with experiment.

## Introduction

Progress in materials science is difficult without reliable computational methods that can predict materials properties with high accuracy. *Ab initio* methods that solve an electronic Hamiltonian are standard techniques for investigating crystalline materials. The main *ab initio* workhorse in solid-state physics, density functional theory (DFT), is a mean field theory. Despite relying upon approximate exchange-correlation functionals DFT results are usually in a good agreement with experiment often because of a cancellation of errors when comparing the energetics of similar systems. When the energies of systems with topologically different electronic structures are compared the DFT results are typically worse. Thus band gaps [1], cohesive energies [2], formation energies of defects [2,3], and predicted thermodynamic stability of different phases [4] typically require post-processing corrections [3-5] to improve their agreement with experiment.

The errors in DFT calculations arise predominantly from the use of approximate exchange-correlation functionals, which are often based on many-body solutions of model systems, e.g. DMC calculations of the homogeneous electron gas [6]. Therefore the direct application of many-body methods to the system of interest should produce results with smaller errors. Quantum chemistry methods, which solve the full many-body Schrödinger equation of molecules, have been in use for several decades [7]. Of these methods coupled cluster theory (CCSD(T)) [8] can often achieve chemical accuracy, i.e. errors in the total energy of less than 1kcal/mol. In a small subset of systems one can solve the Schrödinger equation with full configuration interaction (FCI) [9]. While quantum chemistry methods have been successful for small systems their unfavorable scaling in the number of electrons,  $N$  (within a fixed basis)

is  $N^7$  for CCSD(T) and  $e^N$  for FCI which has severely limited their use in solids. They have only recently been applied to solids in non-converged fashion [10]. The convergence of such approaches is still intractable for many systems of interest.

Another class of techniques – quantum Monte Carlo methods – employs stochastic approaches to numerically solve the many-body Schrödinger equation [11, 12]. Several flavors exist such as auxiliary-field Monte Carlo [13- 15], path-integral Monte Carlo [16], reptation quantum Monte Carlo [17]), variational Monte Carlo (VMC) and diffusion Monte Carlo (DMC). Of these methods applications to solids have mostly been restricted to VMC and DMC, and to a lesser extent auxiliary-field Monte Carlo. Variational Monte Carlo uses an explicitly constructed many-body wave function to evaluate expectation values. This approach is often exploited to optimize a trial wave function for use in more accurate DMC. DMC is a stochastic projector method, which directly solves the many-body Schrödinger equation numerically by evolving in imaginary time from an initial trial wave function towards the ground-state wave function in the infinite-time limit. It has a favorable scaling in the electrons ( $N^3$ - $N^4$ ), with improved scaling possible [18], and scales nearly linearly with the number of computer processors [19,20]. Despite including the full many-body terms of the Schrödinger equation and therefore potentially being more accurate than other methods, DMC relies on several approximations, the most important of which are: the fixed-node (or fixed-phase) approximation, the dependence on supercell size for extended systems, i.e. finite-size effects, and when all-electron calculations are infeasible the use of mean-field based non-local pseudopotentials.

In order to maintain the antisymmetry of the wave function and maintain the stability of the algorithm, the zeros (nodes) of the wave functions are typically fixed in a DMC calculation. This fixed-node approximation is enforced by preventing walker moves in configuration space which change the sign of the trial wave function. Although the final fixed-node wave function will be different from the exact ground-state wave function, the total energy is only quadratic in this difference. Thus it is believed that fixed-node error is small and should not have a sizable effect on materials properties [12]. Moreover the effect of incorrect nodes can be reduced by improving the quality of the trial wave function, for example by using a backflow transformation [21]. The fixed-node formalism deals with real wave functions, but it can be generalized to handle complex wave functions. The fixed-phase approximation [22] has been used to calculate the properties of systems such as quantum dots in a magnetic field [23] and to handle twisted boundary conditions in metals [24, 25]. We will discuss the effect of the fixed-node approximation for the variety of materials presented in this work.

Typically DMC calculations are performed using supercells large enough to contain the exchange-correlation hole. These results usually still require corrections for removing residual size effects. Remaining one-body size effects originating from the kinetic energy term can be corrected either approximately using DFT results, by adding the DFT energy difference between a converged k-point grid calculation and a calculation using the equivalent number of k-points as the supercell used in the DMC calculation, or directly in DMC by employing twist averaging [24]. The former, DFT corrections, has been shown to be insufficient for some metallic systems [25]. To correct for exchange-correlation many-body finite-size effects one can use the model periodic Coulomb interaction [26-28], apply post-processing

corrections of Chiesa [29], KZK [30], or extrapolate to an infinite-sized supercell by performing calculations with different sized supercells.

All-electron DMC calculations are prohibitively expensive due to unfavorable scaling with the atomic number,  $Z$  (from  $Z^{5.5}$  [31] to  $Z^{6.5}$  [32]). In addition the effective speed of the innermost electrons in high- $Z$  elements approaches the speed of light, such that relativistic effects must be included. This cannot be done using the Schrödinger equation and instead requires solving the fully-relativistic Dirac equation, which is not currently possible with state-of-the-art DMC methods. Since the direct relativistic effects on valence electrons are small, a standard way to avoid solving the Dirac equation is to remove the fast-moving core electrons and include their effect on the valence electrons using a relativistic pseudopotential [33] with the Schrödinger equation.

There are two main types of *ab initio* pseudopotentials: 1) energy-consistent pseudopotentials [34] where a model Hamiltonian containing only valence electrons is constructed such that it reproduces the all-electron energies of several reference states, and 2) shape-consistent pseudopotentials [35] in which the pseudoorbitals reproduce the shapes of the all-electron orbital outside of a core region for a chosen reference state. The latter approach is only possible within the one-electron picture and implies that the energies of the all-electron and pseudoorbitals agree. In solid-state physics shape-consistent pseudopotentials are often referred to as norm-conserving pseudopotentials since norm-conservation is imposed, i.e., the charge density integrated over the core region of the all-electron and pseudoorbitals are required to agree [36])

Since DMC-based pseudopotentials are currently unavailable DMC calculations are performed using other types of pseudopotentials. Traditionally Hartree-Fock (HF) (or when including relativity Dirac-Hartree-Fock (DHF)) pseudopotentials have been used in DMC calculations. These pseudopotentials omit correlation between electrons and therefore are believed to be appropriate in cases where core-core and core-valence correlations play a small role. Shape-consistent Dirac-Hartree-Fock based relativistic pseudopotentials containing spin-orbit terms have been developed by Trail and Needs [37,38] based on the Dirac-Coulomb Hamiltonian. The long-range non-local HF or DHF exchange interaction was removed during pseudopotential construction so that the pseudopotentials are non-local only near the core. Trail-Needs (TN) pseudopotentials, which have been developed for use in solids, are tabulated on a grid and have a rather large core, which is beneficial for computing plane-wave based trial wave functions. Energy-consistent pseudopotentials introduced by Burkatzki and coworkers [39,40] (BFD pseudopotentials) have been developed for use in quantum chemistry codes, so they are supplemented with correlation-consistent valence basis set with up to pV5Z quality for the first and the second row main group elements, up to pVTZ for the third to fifth row main group elements and up to pVQZ quality for the 3d transition metals. They are based on the scalar relativistic Wood-Boring Hamiltonian [41], which is however less involved than DHF/DC approach. For 3d transition metals these pseudopotentials have smaller sized cores compared with Trail-Needs pseudopotentials [37,38]. Very recently Trail and Needs introduced correlated electron pseudopotentials which may be considered as a generalization of independent electron norm-conserving pseudopotential theory to the many body one [42,43]. The suggested approach is currently limited to systems that contain only one valence electron therefore, for almost all elements; this restricts the generation of pseudopotentials to ions. Despite this

limitation Trail and Needs showed that the transferability of such pseudopotentials is still high for some systems by demonstrating better agreement with all electron results compared to TN or BFD pseudopotentials.

DMC calculations have also been performed using DFT pseudopotentials, which include the effects of electron correlations in an approximate manner. These shape-consistent pseudopotentials, commonly based on either the local density approximation (LDA) [6,44] or semi-local - generalized gradient approximation (GGA) [45,46] approximations, have been used in DMC to study [47-52] properties of solids. The DMC results with these pseudopotentials often yield better agreement with experiment than DFT calculations for most materials, but DMC yield worse results when compared with DFT calculations that use hybrid exchange-correlation functionals or functionals with van-der-Vaals corrections [50]. No tools exist to construct pseudopotentials with high-level exchange-correlation functionals, as hybrid functionals (PBE0 [45,53], HSE [54], B3LYP [55,56]) or nonlocal functionals (vdw-DF [57]). There is also evidence that HF- or DHF-adjusted PPs give better results in DMC calculations than DFT/LDA-based PP [58,59]. Furthermore the investigation of Russo et al. [60] on several 3d transition metal compounds shows that HF-adjusted pseudopotentials can be also applied in DFT calculations with only small loss of accuracy. In his study of uranyl  $\text{UO}_2^{2+}$  Jong, et al. [61] have shown that good transferability from HF to DFT is achieved only for small core pseudopotentials.

The use of nonlocal pseudopotentials in DMC can change the sign of a walker creating an unstable algorithm similar to the fermion sign problem. A common approach to avoid this instability is to project the nonlocal part of the propagator onto the trial wave function producing a local potential. If the trial wave function closely resembles the fixed-node ground-state wave function, the localization error introduced by this procedure is small and proportional to the square of the difference of these wave functions [62]. The size of this localization error is difficult to estimate. While in the past it has typically been assumed that the localization error is smaller than the fixed-node error [11], we show that for systems containing heavier elements the former not only can be the dominant source of error in the calculation, but it can also lead to unexpected results in calculations and high sensitivity to the details of the calculation and the level of optimization of the trial wave-function. Note that no localization approximation is required in VMC. We will discuss the impact of the localization approximation in DMC on the properties of molecules.

The fixed-node approximation and the use of non-local pseudopotentials in DMC introduce errors, which can be difficult to disentangle. To aid in understanding the impact of these approximations we performed a large set of DMC calculations of different dimers and heteroatomic molecules. We used statistical analysis to elucidate the correlations between these errors and to determine their effect on energetic and spectroscopic properties. We will show how these errors can propagate from molecules to solids and will provide a practical guideline on how to improve the DMC results in solids by employing rather inexpensive calculations on molecules.

Progress in applying DMC methods to a wider range of real materials will benefit from automating wave function optimization, since it is this step in a calculation that typically requires the greatest amount of human time. As we will discuss in the following the careful optimization of the trial wave function is

crucial to reduce the dependence of localization error on the shape of the trial wave function when non-local pseudopotentials are employed. Therefore in this work we provide practical guidelines for generating optimal trial wave functions within a given class of Jastrow-Slater form.

The paper is organized as follows. We begin by describing the methodological aspects of our calculations, followed by a careful analysis of the approximations employed in DMC calculations. Their effect is assessed in several systems. We suggest methods to reduce the approximations associated with the use of non-local pseudopotentials.

## Methodology

We studied a large number of systems containing elements belonging to different blocks of the periodic system (see Tables 1). All calculations presented in this work were performed with the use of pseudopotentials. We applied the Troullier-Martin scheme [63] to construct norm-conserving pseudopotentials with the Opium code [64]. The PBE exchange-correlation functional [45,46] was used for transition and post-transition metals and LDA functional [6,44] was used for all others. Scalar-relativistic effects [65] are included. For transition and post-transition metals several pseudopotentials were produced with different numbers of valence electrons (see Table 1). Pseudopotentials were employed in semi-local form with the Qbox DFT code [66] or within a Kleinman-Bylander formulation [67] with the Quantum Espresso [68] DFT code. Additionally TN pseudopotentials [37,38] and BFD pseudopotentials [39,40] were used for Sn. Several criteria were used to choose a particular local channel for the pseudopotential. First we carefully checked if ghost states were present for a particular choice of the local channel. If ghost states are present we could not employ the Kleinman-Bylander separable form in Quantum Espresso to determine the DFT trial wave function. Next, among the local channels that did not have a ghost state we chose the local channel to be the one that resulted in a trial wave function having the lowest variance of the energy. This allowed us to reduce the DMC calculation time significantly. We have additionally investigated the impact on our DMC results of choosing different channels to be local. In low-Z elements and noble gases we employed Casula’s t-moves [69] in both the molecule and solid calculations for consistency.

Table 1: Some details of the pseudopotentials used in this work. Shown are the names of the element (with an additional designation for elements investigated with more than one pseudopotential), the number of valence electrons per atom, the core-radius (the minimum radius outside of which all of the atomic single-particle pseudo-orbitals and all-electron orbitals agree), the local channel, the code used to produce trial wave functions and the quality of the basis as given by either the kinetic energy cut-off used in plane-wave calculations in Rydberg or by the quality of the Gaussian basis set. The elements are arranged according to the angular momentum of their open shells and their mass in ascending order.

Element	number of valence electrons	core radius, au	Local channel	code	quality
<b>s block</b>					
Li	3	0.60	s	pwscf	450
Be	2	1.30	s	pwscf	240
<b>p block</b>					
B	3	1.30	s	pwscf	200
C	4	1.00	s	pwscf	210
N	5	1.30	s	pwscf	200
F	7	1.00	s	pwscf	180

Al	3	1.78	p	pwscf	150
Si	4	1.70	p	pwscf	150
P	5	1.27	s	pwscf	225
Cl	7	1.14	p	pwscf	360
Sn <sup>TN</sup>	4	2.98	d	pwscf	240
Sn <sup>14</sup>	14	2.47	d	qbox	600
Sn <sup>22</sup>	22	1.80	p	pwscf	900
Sn <sup>BFD</sup>	4		p	molpro	VDZ
<b>d block</b>					
Mo	14	2.00	p	pwscf	500
Rh	17	2.00	p	pwscf	500
Pd	18	2.00	p	pwscf	500
Ag <sup>11</sup>	11	2.00	p	pwscf	240
Ag <sup>19</sup>	19	2.00	p	pwscf	500
Ta	13	2.32	s	pwscf	500
<b>noble gases</b>					
Ar	8	1.12	p	pwscf	220
Kr	8	1.37	p	pwscf	220
Xe	8	1.90	s	pwscf	250

The single-particle DFT/HF orbitals were used to form a DMC trial function composed of a product of a spin-up and spin-down Slater determinants multiplied by a Jastrow factor. Jastrow factor contained one-, two-, and three-body correlation terms [70] with parameters that were optimized by variance minimization [71]. For each of the systems presented we used at least 25,000 VMC configurations in the optimization unless stated otherwise. We did not modify the number of walkers according to the total variance of each atom to get an approximately uniform energy resolution for all studied systems since we found that using 25,000 VMC configurations was sufficient to obtain VMC total energy error bars of better than 0.1 eV/atom for all systems (better than 0.005 eV/atom for Sn<sup>BFD</sup>). Individual DMC calculations were performed using either CASINO [72] or QMCPACK [20,73]. The single-electron Kohn-Sham DFT orbitals were computed self consistently using the PBE approximation for the exchange-correlation functional with a plane-wave basis set. For the DMC calculations these orbitals were transformed into cubic splines [74] on a uniform grid with the grid spacing chosen such that the kinetic energy computed using the plane-wave and the cubic-spline basis set were in close agreement. The plane-wave cutoff used in each DFT calculation (if not mentioned explicitly) was chosen such that both the variance of the trial wave function and the total DFT energy were converged, the latter to within 1 meV/atom. The DMC time step was chosen such that the time-step error was less than the DMC statistical error. For all systems the former are below 0.03 eV per atom.

To achieve a generality in our conclusions we studied various molecules with different bonding mechanisms (see Table 2). In the discussion that follows we will discuss the implications of our investigations for each of these groups. In addition we also compare the DMC results for molecules and solids containing low- and high-Z elements.

For our plane-wave DFT calculations of molecules and atoms we used cubic boxes with box lengths of 20 au for low-Z elements and noble gases and 30 au for transition and post-transition metals. Where possible orbital occupations were chosen to agree with experimentally observed ground-state

multiplicities (see Table 2). For the aluminum dimer it was not possible to stabilize the  $^3\Pi_u$  ground state within DFT, so we used the  $^3\Sigma_g^-$  state and compared against experimental values for the same configuration.

Calculations of solid phases has been performed with 32 atoms in a supercell for BN, BP, C, LiCl, LiF, SiC, Si, 28 atoms for Li, 66 atoms for Be, 108 atoms for Al, Ar, Kr, Xe, 27 atoms for Ag, Mo, Pd, Rh, Ta and 54 atoms for Sn. The residual finite-size effects have been corrected using several methods. One-body-finite-size effects were corrected by employing twist-averaged boundary conditions [24]. For low-Z elements and the noble gases the remaining two-body finite-size errors have been accounted for by using MPC [26,75] and the Chiesa correction [29]. For the transition and post-transition metals the remaining many-body finite-size effects were included using the KZK correction [30].

To obtain the bonding curve of molecules and the equation of state (EOS) of solids DMC calculations were performed for a range of molecule spacings,  $R$ , and solid lattice parameters,  $a_{\text{lat}}$ , within about 5% of the energy minimum. The resulting energies of the diatomic molecules were fit to a Morse potential [76]:

$$E(R) = D_e + E_D(1 - e^{-\alpha(R-R_e)})^2 \quad (1),$$

where  $E_D$  is the dissociation energy of the rigid molecule,  $R_e$  is the optimal bond length, and the constant  $\alpha$  were all found by minimizing the sum of squares of the deviations. The spectroscopic constants were determined by

$$w_e = \frac{\alpha\sqrt{2E_D/\mu}}{2\pi c} \quad (2),$$

$$w_e x_e = w_e^2 \frac{hc}{4E_D} \quad (3),$$

$$D_e = E_D - \frac{1}{2}w_e \quad (4),$$

where the speed of light  $c$  is used to express spectroscopic constants in the units of  $\text{cm}^{-1}$ . An example of DMC computed energies as a function of the bond length for an  $\text{Sn}_2$  dimer using the  $\text{Sn}^{\text{TN}}$  pseudopotential together with a fitted Morse potential is shown in Fig. 2a.

The energies of fcc Ag19, fcc Pd, fcc Rh, bcc Mo and bcc Ta were fitted to a Murnaghan equation of state [77]:

$$E(V) = E_0 + B_0 V_0 \left( \frac{1}{B'_0(B'_0-1)} \left( \frac{V}{V_0} \right)^{1-B'_0} + \frac{1}{B'_0} \frac{V}{V_0} - \frac{1}{B'_0-1} \right) \quad (5),$$

where  $V_0$  is the equilibrium volume,  $B_0$  is the bulk modulus, and  $B'_0$  is the first derivative of the bulk modulus at the equilibrium volume. The energies of all other solids were fitted to a Vinet equation of state (EOS) [78]:



$$E(V) = E_0 + \frac{4B_0V_0}{(B'_0-1)^2} - 2V_0B_0(B'_0-1)^{-2}(5 + 3B'_0(V-1) - 3V)e^{\left(-\frac{3}{2}(B'_0-1)(V-1)\right)} \quad (5).$$

The fits to the nonlinear equations (1) and (5) were performed using bootstrapping method [79] with the errors in the fitting parameters corresponding to a one sigma (0.682) confidence interval. The results for the diatomic molecules are presented in Table 2 and for the solid calculations in Table 3.

Table 2: Spectroscopic constants of molecules obtained from DFT, DMC, and experiment. Statistical errors bars are given in parenthesis and include the effect of statistical uncertainties of DMC energies. If available the experimental error bars are given in parenthesis. The molecules are arranged according to the type of bonding and total mass (in ascending order).

Element	Term symbol	method	$R_e, \text{\AA}$	$D_e, \text{eV}$	$w_e, \text{cm}^{-1}$
s-s bonding					
Be <sub>2</sub>	$^1\Sigma_g$ (GS)	LDA	2.389	0.563	348
		DMC	2.432(4)	0.184(2)	263(5)
		Exp.	2.460 <sup>d</sup>	0.0867 <sup>d</sup>	
Li <sub>2</sub>	$^1\Sigma_g^+$ (GS)	LDA	2.715	1.026	317.6
		DMC	2.719(4)	0.957(2)	327(5)
		Exp.	2.6733 <sup>d</sup>	1.00362 <sup>d</sup>	351.4066 <sup>d</sup>
s-p bonding					
LiF	$^1\Sigma^+$ (GS)	LDA	1.546	6.783	907
		DMC	1.5551(7)	6.126(4)	950(2)
		Exp.	1.56386 <sup>d</sup>	5.9654 <sup>d</sup>	910.57 <sup>d</sup>
LiCl	$^1\Sigma^+$ (GS)	LDA	2.009	5.221	617
		DMC	2.0212(9)	5.023(3)	646(2)
		Exp.	2.02067 <sup>d</sup>	4.9016 <sup>d</sup>	642.95 <sup>d</sup>
p-p bonding					
C <sub>2</sub>	$^1\Sigma_g^+$ (GS)	LDA	1.263	6.998	1607
		DMC	1.2563(7)	5.678(4)	1834(6)
		Exp.	1.243 <sup>d</sup>	6.2186 <sup>d</sup>	1855.066 <sup>d</sup>
BN	$^3\Pi$ (GS)	LDA	1.333	5.73	1436
		DMC	1.3156(4)	4.463(3)	1540(3)
		Exp.	1.325 <sup>d</sup>	4.8712 <sup>d</sup>	1514.6 <sup>d</sup>
BP		LDA	1.736	4.600	916
		DMC	1.7196(2)	3.517(3)	990(1)
		Exp.		3.596 <sup>h</sup>	
SiC	$X^3\Pi$ (GS)	LDA	1.712	5.44	919.1
		DMC	1.6989(9)	4.456(3)	1000(3)
		Exp.	1.732 <sup>f</sup>	4.63 <sup>d</sup>	954.2 <sup>f</sup>
Al <sub>2</sub>	$^1\Sigma_g^-$ ( $^3\Pi_u$ -GS)	LDA	2.456	2.035	315
		DMC	2.426(3)	1.440(3)	369(5)
		Exp.	2.466 <sup>b</sup>	1.3255 <sup>b</sup>	350.01 <sup>b</sup>
Si <sub>2</sub>	$^3\Sigma_g^-$ (GS)	LDA	2.262	4.025	459
		DMC	2.20(2)	3.36(1)	545(51)
		Exp.	2.246 <sup>d</sup>	3.2267 <sup>d</sup>	510.98 <sup>d</sup>
Sn <sub>2</sub> <sup>TN</sup>	$^3\Sigma_g^-$ (GS)	PBE	2.762	2.837	181
		DMC	2.818(5)	2.358(7)	182(3)
		Exp.	2.748 <sup>g</sup>	1.939 <sup>h</sup>	189 <sup>p</sup>
Sn <sub>2</sub> <sup>14</sup>	$^3\Sigma_g^-$ (GS)	PBE	2.79	2.52	161
		DMC	2.668(8)	2.03(3)	188(2)
		Exp.	2.748 <sup>g</sup>	1.939 <sup>h</sup>	189 <sup>p</sup>
Sn <sub>2</sub> <sup>22</sup>	$^3\Sigma_g^-$ (GS)	PBE	2.807	2.619	158
		DMC	2.750(6)	2.31(2)	180(3)
		Exp.	2.748 <sup>g</sup>	1.939 <sup>h</sup>	189 <sup>p</sup>
Sn <sub>2</sub> <sup>BFD</sup>	$^3\Sigma_g^-$ (GS)	HF	2.752	0.829	203.3

		DMC	2.782(3)	2.287(4)	191(3)
		Exp.	2.748 <sup>g</sup>	1.939 <sup>h</sup>	189 <sup>p</sup>
d-d bonding					
Mo <sub>2</sub>	<sup>1</sup> Σ <sub>g</sub> <sup>+</sup> (GS)	PBE	1.916	3.941	534
		DMC	1.909(2)	2.94(1)	549(2)
		Exp.	1.929 <sup>e</sup>	4.476 <sup>i</sup>	477.1 <sup>e</sup>
Rh <sub>2</sub>	<sup>5</sup> Δ <sub>g,u</sub> (GS)	PBE	2.200	3.29	317
		DMC	2.195(5)	1.97(1)	322(6)
		Exp.		2.9 <sup>l</sup>	283.9 <sup>o</sup>
Pd <sub>2</sub>	<sup>3</sup> Σ <sub>u</sub> <sup>+</sup> (GS)	PBE	2.469	1.347	196
		DMC	2.463(6)	0.54(1)	217(5)
		Exp.		1.03 <sup>k</sup>	210 <sup>n</sup>
Ag <sub>2</sub> <sup>11</sup>	<sup>1</sup> Σ <sub>g</sub> <sup>+</sup> (GS)	PBE	2.612	1.699	172
		DMC	2.456(5)	1.61(3)	228(3)
		Exp.	2.5335 <sup>a</sup>	1.688 <sup>h</sup>	192.4 <sup>m</sup>
Ag <sub>2</sub> <sup>19</sup>	<sup>1</sup> Σ <sub>g</sub> <sup>+</sup> (GS)	PBE	2.560	1.787	174
		DMC	2.552(7)	1.54(2)	190(3)
		Exp.	2.5335(5) <sup>a</sup>	1.688 <sup>h</sup>	192.4 <sup>m</sup>
Ta <sub>2</sub>	<sup>1</sup> Σ <sub>g</sub> <sup>+</sup> (GS)	PBE	2.13	4.22	293
		DMC	2.111(2)	3.297(9)	330(5)
		Exp.		4(1) <sup>h</sup>	300.2 <sup>q</sup>
Van der Waals bonding					
Ar <sub>2</sub>	<sup>1</sup> Σ <sub>g</sub> <sup>+</sup> (GS)	LDA	3.420	0.030	51.6
		DMC	3.75(1)	0.011(3)	32(1)
		Exp.	3.7565 <sup>c</sup>	0.01234 <sup>c</sup>	30.9 <sup>c</sup>
Kr <sub>2</sub>	<sup>1</sup> Σ <sub>g</sub> <sup>+</sup> (GS)	LDA	3.715	0.037	35.2
		DMC	4.05(1)	0.0156(8)	22.6(7)
		Exp.	4.008 <sup>c</sup>	0.017336 <sup>c</sup>	23.6 <sup>c</sup>
Xe <sub>2</sub>	<sup>1</sup> Σ <sub>g</sub> (GS)	LDA	4.143	0.042	26.8
		DMC	4.64(5)	0.022(3)	16(2)
		Exp.	4.3627 <sup>c</sup>	0.024323 <sup>c</sup>	20.9 <sup>c</sup>

Ref. a is from [80], b from [81], c from [82], d from [83], e from [84], f from [85], g from [86], h from [87], i from [88], k from [89], l from [90], m from [91], n from [92], o from [93], p from [94], q from [95].

Table 3: Equation of state parameters of solids, the equilibrium lattice constant (alat), the cohesive energy ( $E_{\text{coh}}$ ), and bulk modulus (B) computed using DMC and compared with experiment. The remaining data is available in [51] (for Ag<sup>19</sup>, Mo, Pd, Rh, Ta), [50] (for Al, Ar, Be, BN, BP, C, Kr, Li, LiCl, LiF, Si, SiC, Xe) and [52] (for Sn<sup>22</sup>). DMC errors are given in parenthesis in the first row. Experimental values were corrected for finite-temperature and zero-point energy contribution [96] and are shown on the second row.

Element	Structure	Method	alat, Å	$E_{\text{coh}}$ , eV	B, GPa
Ag <sup>11</sup>	fcc	DMC	4.01(2)	3.88(2)	136(72)
		Exp.	4.070 <sup>b</sup>	2.96 <sup>a</sup>	105.7 <sup>a</sup>
Sn <sup>TM</sup>	diamond	DMC	6.673(3)	3.179(4)	40(2)
Sn <sup>14</sup>	diamond	DMC	6.37(5)	2.61(2)	38(14)
		Exp.	6.477 <sup>b</sup>	3.16 <sup>a</sup>	53 <sup>c</sup>

Ref. a is from [97], b from [98], c from [99].

## Results and discussion

a. Localization error

A common method for dealing with nonlocal pseudopotentials within DMC is to use the localization approximation [62]. This introduces a non-systematic localization error ( $err^{loc}$ ) which depends on both the nodes and the detailed shape of the trial wave function which is related to the total DMC energy ( $E_{nl}^{DMC}(\text{nodes, shape})$ ) by the equation:

$$E_{nl}^{DMC}(\text{nodes, shape}) = E_0^{DMC}(\text{nodes}) + err^{loc}(\text{nodes, shape}) \quad (6),$$

where  $E_0^{DMC}$  is the hypothetical total energy from a DMC calculation without the locality approximation. Note that  $E_0^{DMC}$  and  $E_{nl}^{DMC}$  are equal when the trial wave function is equal to the DMC wave function since the localization error is zero. If the trial wave function is sufficiently close to the ground state wave function the localization error is proportional to the square of difference of the wave functions [62].

Figure 1 illustrates the impact that the quality of the Jastrow and the localization error can have on a DMC total energy curve when using a standard DFT norm-converging Troullier-Martins pseudopotential. This figure contains total energies for the Ag dimer as a function of bond length computed using three levels of approximation. The HF and VMC curves correspond to the expectation values of the Hamiltonian with and without the optimized Jastrow term included,  $\langle D | \mathcal{H} | D \rangle$  and  $\langle De^J | \mathcal{H} | De^J \rangle$  respectively, where  $De^J$  denotes the many-body Slater-Jastrow trial wave function used in the DMC calculation. The smoothness of the HF curve implies that the orbitals, which are taken from separate DFT calculations at each bond length, vary smoothly with bond length and implies that the nodes which arise only from the Slater determinant vary smoothly as well. To compute the VMC curve the Jastrow term was optimized separately at each bond-length. The character of the VMC curve shows that the quality of the Jastrows varies and depends on bond-length since HF results show that the Slater determinant term varies smoothly. Note that in a VMC calculation there is no locality approximation. The unphysical changes seen in the DMC energy as a function of bond length indicate that variations in the quality of the Jastrow can have a large impact on the total energy through the locality approximation. This is particularly pronounced in this system when using the Ag 11 valence pseudopotential because of the large size of the non-local energy term relative to the total energy.

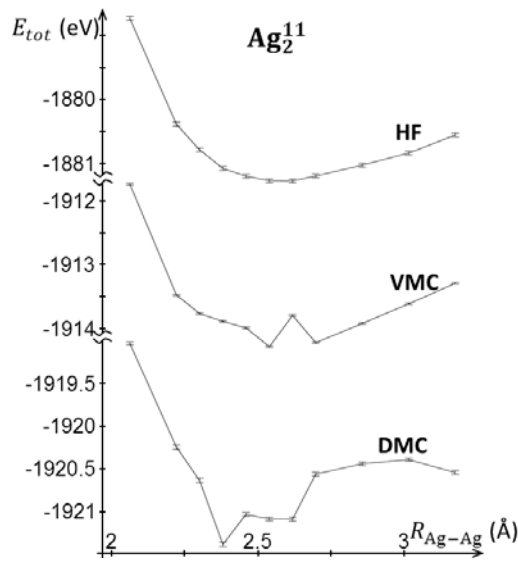


Fig. 1: Effect of Jastrow and localization error on VMC and DMC energy vs bond length curves for the  $\text{Ag}_2$  dimer using the  $\text{Ag}^{11}$  pseudopotential. The HF and VMC correspond to the expectation values of the Hamiltonian with and without the Jastrow term included,  $\langle D | \mathcal{H} | D \rangle$  and  $\langle \text{De}^J | \mathcal{H} | \text{De}^J \rangle$  respectively, where  $\text{De}^J$  denotes the many-body Slater-Jastrow trial wave function.

The variation from smoothness in the DMC curve of Figure 1 gives an estimate of the size of the localization error in the  $\text{Ag}_2$  dimer for the particular set of Jastrows that were obtained from VMC optimization performed at different bond lengths. An alternative method to estimate the localization error at a specific atomic configuration (e.g. one bond length in the dimer) would be to generate a distribution of Jastrows, fixing the Slater determinant and thus the nodes, and compute the corresponding distribution of DMC total energies. For a given Jastrow accuracy, which is related to 1) its functional form, 2) the number of parameters optimized, 3) the number of electronic configurations used in sampling, and 4) the robustness of the algorithm for finding global minima, one would expect the spread of DMC energies to increase with the size of the localization error. In order to generate a large number of Jastrow functions in a realistic time frame we instead performed this analysis for a Sn atom using a Trail-Needs pseudopotential,  $\text{Sn}^{\text{TN}}$ , which has only 4 valence electrons. Starting with a fixed functional form and an initial set of parameter values the parameters in the Jastrow were iterated using variance minimization until an equilibration in the total VMC energy and variance became apparent. Note that in the optimization a hard limit was placed on the total change that the parameters are allowed to evolve in each iteration. Following equilibration the Jastrow generated after each successive iteration was used to compute DMC total energies.

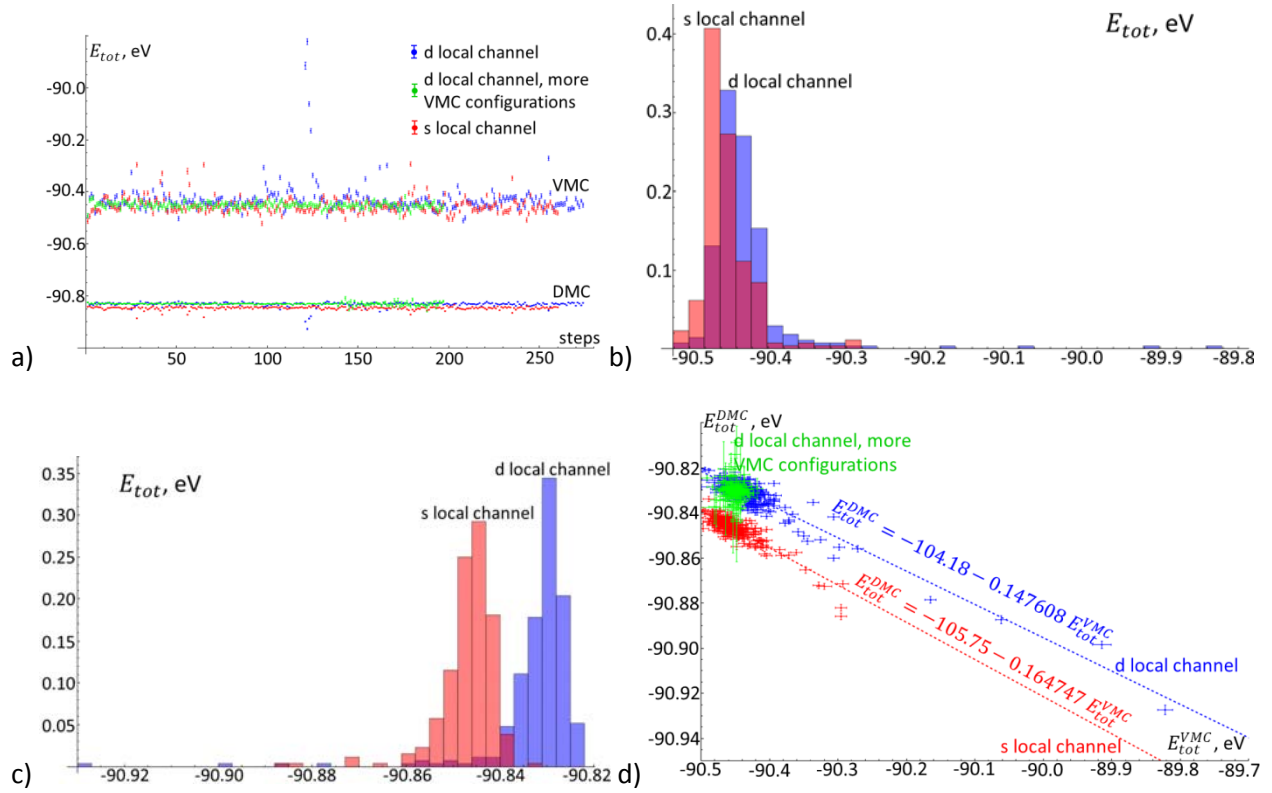


Fig. 2: (a) Total energies from VMC (upper values) and DMC (lower values) calculations for  $\text{Sn}^{\text{TN}}$  atom in its ground state using different values of the parameters in the Jastrow term. (b) Histogram of VMC total energies. (c) Histogram of DMC total energies. (d) Correlation between VMC and DMC total energies.

Shown in Fig. 2a are the VMC and DMC energies for the Sn atom after each iteration during the optimization. The initial equilibration iterations are not shown. Separate results are plotted corresponding to the choice of using either s or d as the local angular momentum channel. For the case of the d local channel optimizations were performed using 10,000 and 100,000 electronic configurations for comparison. The distribution of VMC energies has a well-pronounced non-symmetric profile (Fig. 2b), which is a result of the optimization procedure. Note that the statistical uncertainty of each VMC energy (on the order of the size of symbols in Fig. 2a) is much smaller than the distribution of VMC energies, so that the distribution is mainly the result of variations in the parameters in the Jastrow. Note also that there are several outliers with large VMC energies but that there are no outliers with energies significantly lower than median of the calculations. This is consistent with the variational principle in VMC and demonstrates that the VMC energy is bounded from below. This bound is the lowest VMC energy that can be achieved with a given Slater determinant and a given functional form of the Jastrow (in this case consisting of a linear combination of homogeneous electron-electron, electron-nucleus and electron-electron-nucleus terms in the exponential). When the number of VMC configurations is small larger fluctuations of VMC energies are observed. The distribution of VMC total energies is reduced when we increase the number of VMC configurations from 10,000 to 100,000 as shown in Fig. 2d.

The DMC total energies using the trial wave functions obtained from each VMC calculation are plotted in Fig. 2a. Their distribution (Fig. 2c) like the VMC energies is non-symmetric, but its outliers are below the

median, with no significant outliers above suggesting that it is bounded from above. However the spread of the DMC distribution is one order of magnitude smaller than that of VMC distribution. In Fig. 2d we plot the pairs of VMC and DMC total energies for each trial wave function. There is a clear correlation between them. In the limit that either the non-local term in the Hamiltonian is taken to zero or the VMC optimized Jastrow converges to the “DMC Jastrow” the DMC total energies will depend only on the nodes of the wave function and the distribution of DMC energies will have the width on the order of statistical uncertainty of DMC energy. Note that the statistical uncertainty of the DMC total energies is much smaller than the size of the distribution. The wider distribution of DMC energies therefore can be only attributed to the localization error and its spread provides a lower-bound estimate for this error. In this system the localization error results in the anticorrelation between the VMC and DMC total energies: the wave function which is close to the ground state yields a lower VMC total energy and higher a DMC total energy. The calculations using the s local channel have a slightly smaller spread than the d local channel calculations. This can be attributed to a slightly lower variance of the local energy (see Table 4). The localization error here leads to DMC energies, which do not satisfy the variational principle. The nonlocal energy in the VMC and DMC calculations for the case of the s local channel constitutes -2% of the total energy, which is much smaller than in the case of d local channel (15%). Despite this large difference in the size of the nonlocal energy the impact of the localization error on the anticorrelation of the VMC and DMC energies is not affected.

Table 4: Effect of different local channels on the results of VMC calculations of  $\text{Sn}^{\text{TN}}$  atom. Shown is the local channel, the VMC total energy, variance and nonlocal energy in atomic calculations.

Local channel	$E_{\text{VMC}}, \text{Ha}$	$\text{Var}, \text{Ha}$	$E_{\text{nl}}, \text{Ha}$
s	-2461(1)	14.4(8)	46(1)
p	-2461(1)	16(1)	-103(3)
d	-2460(1)	17.7(35)	-378(5)

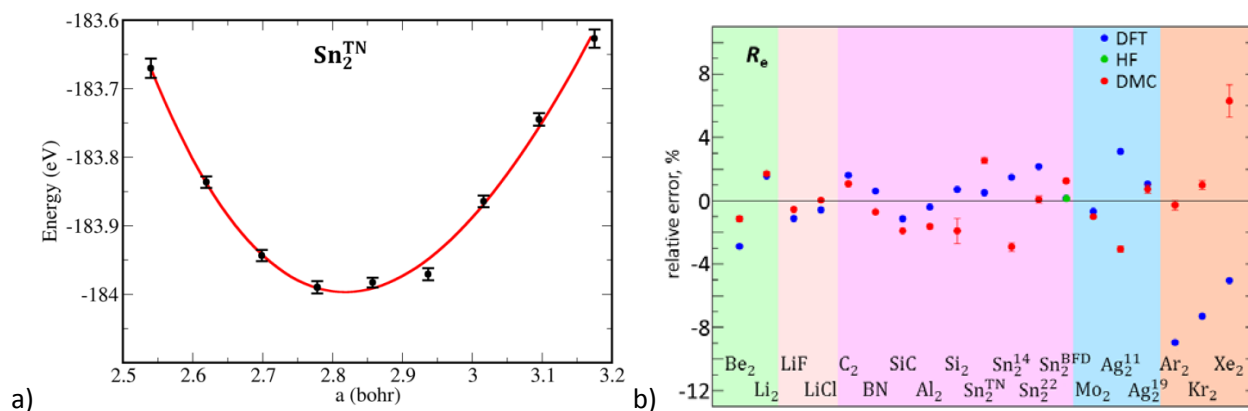
In the  $\text{Sn}^{\text{TN}}$  atom we find that the dependence of localization error on shape of the trial wave function is not affected by the choice of the local channel. To reduce the localization error using a fixed Slater determinant term one should use the largest practical number of electronic configurations during VMC optimization and the most general form of Jastrow. This procedure will produce the narrowest distribution of VMC energies. The trial wave function with the lowest VMC total energy should be chosen (provided its variance is comparable with others). This trial wave function yields an energy that is closest to the lower boundary VMC total energy and correspondingly a DMC energy that is closest to the boundary DMC total energy. When the energies of different systems are compared this procedure will lessen the impact of the shape of the wave function on the total energy, assuring that their energy difference will depend mainly on the nodes of the trial wave functions.

#### b. Effect of the correlation between core and valence electrons

All pseudopotentials used in this work were created using mean-field theories – PBE-DFT or HF. Pseudopotentials constructed using PBE-DFT include only an approximate treatment of the core-valence exchange-correlation contribution, while HF based pseudopotentials include an exact treatment of

exchange but neglect correlation completely. In an attempt to understand how this impacts our DMC results we compared DFT, HF, and DMC calculations obtained using the same form of pseudopotential for a range of molecules.

We first discuss the accuracy of using pseudopotential based DFT-PBE or HF calculations for computing the properties of molecules. The deviation from experiment of several spectroscopic parameters of molecules computed using DFT and HF is shown in Fig. 3. The mean absolute percentage error (MAPE) from experiment of the DFT/HF calculations for the optimal bond length ( $R_e$ ) is 2.16 %, and 14.06% for the spectroscopic constant ( $\omega_e$ ). The mean absolute error (MAE) from experiment of the DFT/HF calculations for the dissociation energy ( $D_e$ ) is 0.50 eV. To investigate the effect of different pseudopotential cores we computed the properties of the  $\text{Sn}_2$  dimer using several different pseudopotentials. These included the Trail-Needs [37,38] and BFD [39,40] Hartree-Fock based pseudopotentials with 4 valence electrons, and the PBE-based pseudopotentials with 14 ( $\text{Sn}^{14}$ ) and 22 ( $\text{Sn}^{22}$ ) valence electrons. In our DFT calculations for  $\text{Sn}_2$  we found that promoting more electrons to the valence (and correspondingly the reduction of the core radius) did not improve agreement with experiment. The employment of the same level of theory for pseudopotential construction and for dimer calculations (e.g. DFT for  $\text{Sn}^{22}$  and HF for  $\text{Sn}^{\text{BFD}}$  pseudopotentials) also does not improve the agreement with experiment compared to the DFT results using the pseudopotentials constructed with a different level of theory (e.g. HF for  $\text{Sn}^{\text{TN}}$  and  $\text{Sn}^{\text{BFD}}$ ). Furthermore, pseudopotentials constructed with the same level of theory with the same number of valence electrons ( $\text{Sn}^{\text{TN}}$  and  $\text{Sn}^{\text{BFD}}$ ) yielded substantially different DFT results. DFT calculations fall short in predicting the properties of noble gases. The optimal bond distance is largely underestimated and the spectroscopic constant  $\omega_e$  is largely overestimated. The DFT-computed dissociation energy is overestimated compared to experiment for all studied molecules except for  $\text{Mo}_2$ .



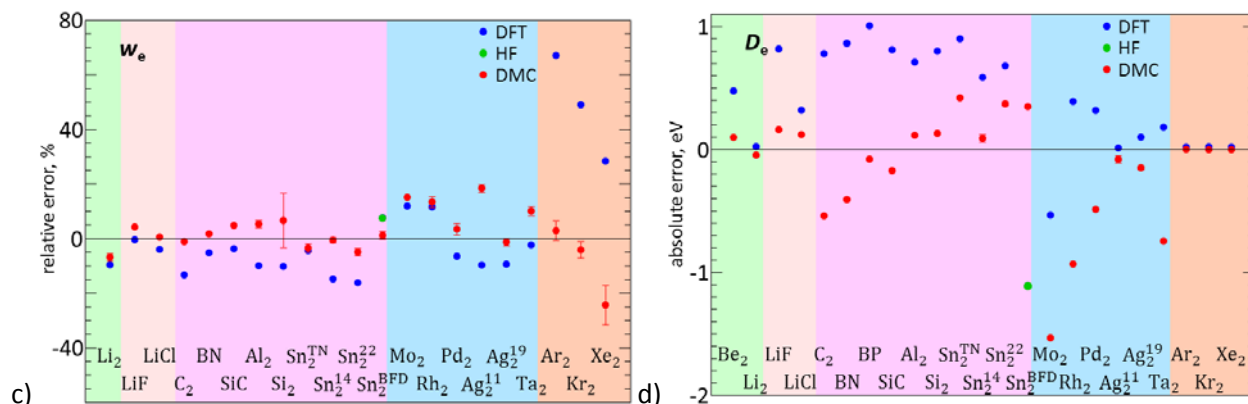


Fig. 3: (a) Energy of  $Sn_2^{TN}$  dimer as a function of its length (DMC energies with statistical error bars are given by black symbols, fit to Morse potential – by red curve). (b) Deviations of DFT and DMC computed parameters from experiment for optimal bond length  $R_e$ , (c) spectroscopic constant  $w_e$  and (d) dissociation energy  $D_e$ . The molecules in b), c) and d) are grouped by bonding mechanism – s-s (green background), s-p (red), p-p (magenta), d-d (blue), van der Waals (brown) – and by total mass in ascending order.

We performed DMC calculations for each molecule using trial wave functions composed of the same orbitals and the same pseudopotential that were used in the DFT/HF calculations. The deviations of these DMC-computed spectroscopic parameters from experiment are shown in Fig. 3. There appears to be no similarity between DFT/HF and DMC deviations from experiment. The errors can even have different signs. Compared to experiment the DMC calculations gave MAPE of 1.57 % for  $R_e$  and 6.41% for  $w_e$  and MAE of 0.31 eV for  $D_e$ . In the case of Sn and Ag the inclusion of more electrons in valence improved the agreement with experiment. We suspect that the inclusion of more electrons in valence which results in a decrease of the core-valence electron density overlap (see Fig. 4) will reduce the impact of the neglected correlation between the core and valence electrons in the DMC calculations which makes these pseudopotentials more appropriate for DMC. There will also likely be a reduction in the localization error when the number of valence electrons are increased provided the cutoff radii are chosen to be smaller because there will be a smaller region around each atom that will be impacted by the localization approximation. Foyevtsova, et al. [100] found that increasing the number of valence electrons when constructing a Cu pseudopotential (using a hard Ne-core pseudopotential) beyond what was required for converged DFT results was necessary to obtain good results in DMC. Our DMC calculations perform uniformly well across all groups of molecules. There is however a tendency to underestimate dissociation energy of molecules with d-d bonding.



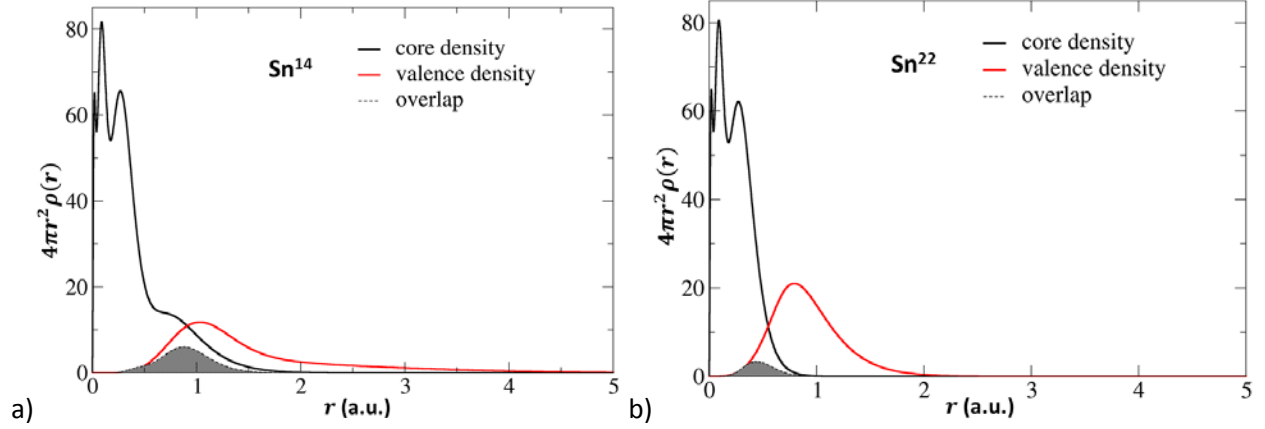


Fig. 4: Core and valence electronic density as a function of distance from the nucleus in (a)  $\text{Sn}^{14}$  and (b)  $\text{Sn}^{22}$  pseudopotentials.

Table 5: Effect of different procedures to improve the nodes of the trial wave function for DMC calculations. The variance listed for each case is for dimer at the closest to optimal bond length.

Dimer	Comment	Var, au	Re, Å	De, eV	we, cm-1
	no backflow	0.13(1)	2.818(8)	2.358(9)	172(81)
	with backflow	0.064(9)	2.77(1)	2.34(1)	176(41)
	no backflow	1.61(3)	2.7(1)	2.0(2)	178(94)
	with backflow	1.23(3)	2.93(9)	5.3(2)	156(389)
	no backflow	3.2(1)	2.75(1)	2.31(2)	170(86)
	with backflow	1.88(9)	2.74(5)	2.25(5)	160(321)
	no backflow	0.041(5)	2.782(2)	2.287(3)	181(19)
	with backflow	0.022(1)	2.786(6)	2.283(7)	178(50)
	no backflow, Ecut=240 Ry	2.23(9)	2.46(7)	1.6(1)	216(80)
	no backflow, Ecut=500 Ry	2.15(6)	2.552(9)	1.54(2)	180(25)
	with backflow, Ecut=500 Ry	1.03(2)	2.53(3)	1.51(3)	191(65)
	no backflow, Ecut=500 Ry	0.83(3)	1.909(2)	2.94(2)	520(11)
	with backflow, Ecut=500 Ry	0.47(2)	1.915(3)	3.22(2)	508(18)
	no backflow, Ecut=240 Ry	1.08(5)	1.915(4)	2.96(2)	513(23)
	with backflow, Ecut=240 Ry	0.65(4)	1.910(3)	3.29(2)	520(48)

#### b. Fixed-node error

Having demonstrated the importance of the choice of the pseudopotential that is used in DMC calculations of molecular properties, we performed a series of calculations to estimate the effect of the fixed-node approximation. The nodes of the trial wave function were changed by incorporating backflow [101] for the  $\text{Sn}_2$ ,  $\text{Ag}_2$ , and  $\text{Mo}_2$  dimers and by increasing the kinetic energy cut-off used in the DFT calculation of the single-particle orbitals, which appear in the determinants of the  $\text{Mo}_2$  dimer trial wave function. For each system the backflow transformation consisted of a homogeneous electron-electron (employing expansion order of 8) and electron-nucleus terms (expansion order of 6), and an inhomogeneous electron-electron-nucleus term (electron-nucleus and electron-electron expansion order of 3). Together with cut-off radii this resulted in a total number of 220 optimizable parameters. The backflow parameters were determined using VMC optimization with variance minimization. The employment of backflow changed the nodal surface as can be seen on Fig. 5a. Table 5 gives the parameters and results of these calculations. Adding backflow and increasing the plane-wave cutoff

reduces the variance of the atoms and dimers. The increase of the kinetic energy cut-off did not significantly affect the total energy of the system in DFT, but reduced the variance of the trial wave function for Mo by 23% in VMC. Applying the backflow transformation reduced the variance of Mo by  $\approx 43\%$  and of Sn by a factor of  $\approx 2$  when using the  $\text{Sn}^{\text{BFD}}$  pseudopotential. We were unable to optimize both the Jastrow and the coefficients of the backflow transformation in case of  $\text{Ag}^{11}$  so no results are reported for this system. In the case of the  $\text{Sn}^{14}$  pseudopotential we encountered instabilities while optimizing the trial wave function that resulted in fluctuating VMC and DMC energy curves like that obtained for  $\text{Ag}_2$  using an 11-valence pseudopotential with DMC shown in Fig. 1. Fitting the curves produced unreasonable spectroscopic properties for the dimer. We assume that such strong fluctuations of DMC energy are due to very high localization error in this pseudopotential that probably results from a large overlap of the valence and core electronic densities (as shown in Fig. 4a).

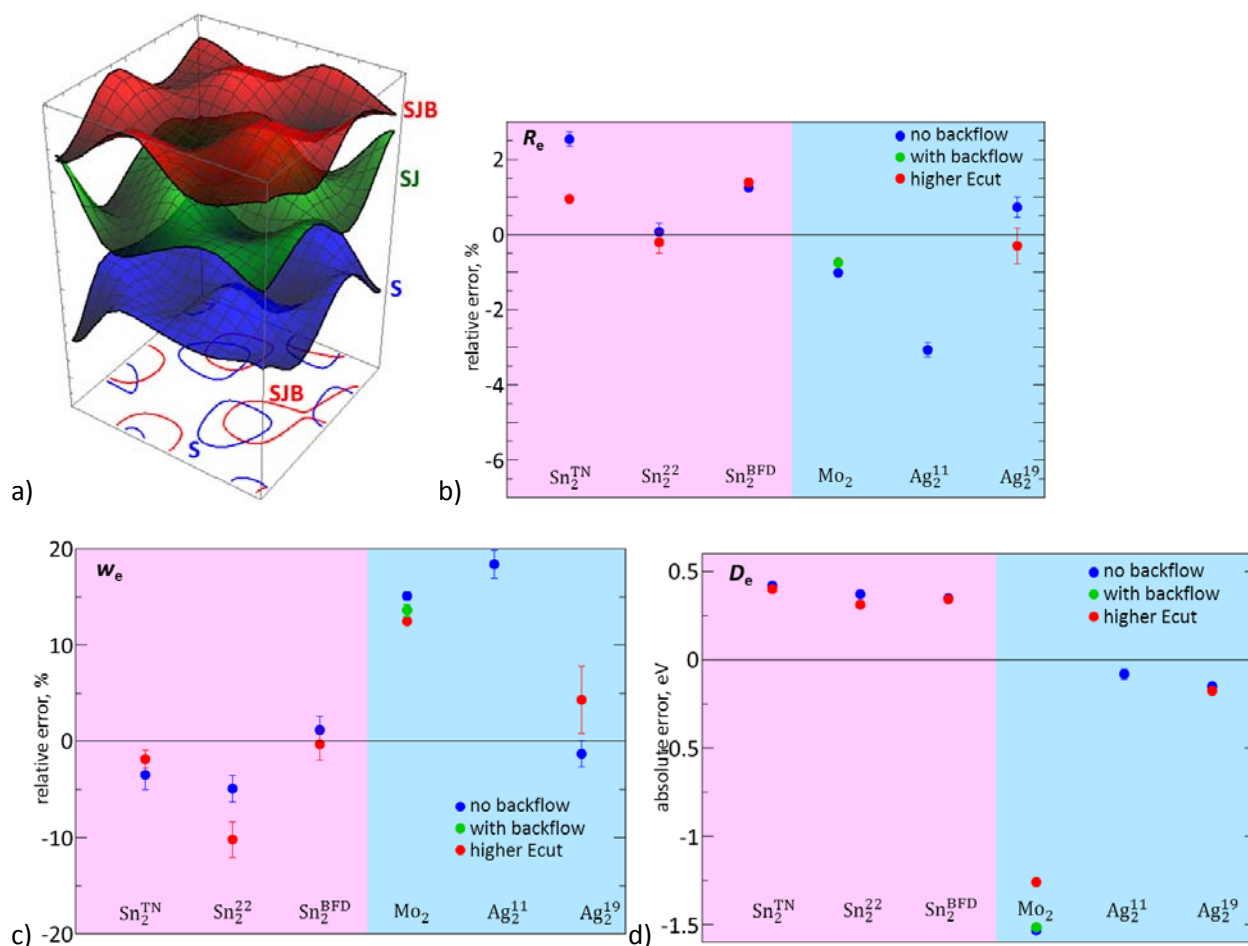


Fig. 5: A projection of the trial wave function and its nodes for the  $\text{Mo}_2$  dimer moving one electron in the basal plane for the Slater only (S), Slater-Jastrow (SJ), and Slater-Jastrow + backflow (SJB) trial wave functions. The nodes of wave function are modified by the backflow transformation (a). Deviations from experiment of DMC computed spectroscopic parameters of dimers employing different nodal structures of the trial wave function: (b) the optimal bond length  $R_e$ , (c) the spectroscopic constant  $w_e$ , and (d) the dissociation energy  $D_e$ . The molecules in b), c) and d) are grouped by bonding mechanism p-p (magenta), and d-d (blue) – and by total mass in ascending order.

The deviations from experiment for different pseudopotentials, different kinetic cut-off energies and for the calculations with/out backflow transformation in DMC are shown in Fig 5. In these systems the effect of changing the nodes of the trial wave function by including backflow had a smaller effect on the calculated properties than changing the pseudopotential.

### c. Correlation between solids and molecules

To determine if it is the fixed-node approximation or it is the use of (and particular choice of) non-local pseudopotentials that has a larger impact on the errors one obtains from DMC simulations we performed calculations of the EOS parameters of the ground-state phase of each solid corresponding to each diatomic molecule listed in Table 2 using the same pseudopotentials. We would expect that the character and thus the corresponding error associated with the nodal structure of the trial wave functions would usually be different in solids compared to diatomic molecules. The fact that we observe such a strong correlation between the errors in calculated quantities for solids and molecules across a wide variety of elements and pseudopotentials despite the potential for completely different fixed-node errors suggests that the error due to the non-local pseudopotential is currently the factor imposing the dominant limitation on the accuracy of our calculations.

There is an additional source of error that arises when DMC is applied to solids – the finite-size effects. Using twist averaging combined with a KZK correction or extrapolation to infinite-sized simulation cells can largely diminish its effects. Therefore in the following our calculations of solids include these corrections. Some of these results have been taken from the work of Shulenburger et al. [50], Hood et al. [51] and Nazarov et al. [52]. The others are given in the Table 3.

To compare our results between each solid and its corresponding diatomic molecule we plotted parameters of the equation of state for the solids against similar parameters describing the energy as a function of molecular length (see Fig. 6). The lattice parameter in each solid, which is proportional to the nearest neighbor equilibrium spacing, is plotted against the optimal bond length of each corresponding diatomic molecule. The energetics of the systems are compared by plotting the cohesive energy of the solid versus the dissociation energy of the molecule. The parameters which describe the curvature of the energy as a function of atomic spacing are the bulk modulus ( $B$ ) for the solid and the spectroscopic parameter  $w_e$  for the molecules.

Before analyzing the correlations between our DMC results of solids and molecules we need to remark about the uncertainties in our DMC results and effects which are not directly included. We start with the statistical uncertainties of the DMC calculations. Vibrational properties have the biggest errors as the curvature depends strongly on statistical uncertainties of our data. The geometrical properties have smaller statistical error bars. The smallest statistical uncertainties correspond to binding energies. When one compares DMC results with experiment it should be noted that there are effects present in experiment – finite-temperature and zero-point energy – which are not included in our DMC calculations. To avoid comparing results obtained at different conditions we used experimental values extrapolated to zero temperature whenever possible. Additionally the zero-point energy was taken into account by subtracting a theoretical estimate of this term from the experimental cohesive energy [96].

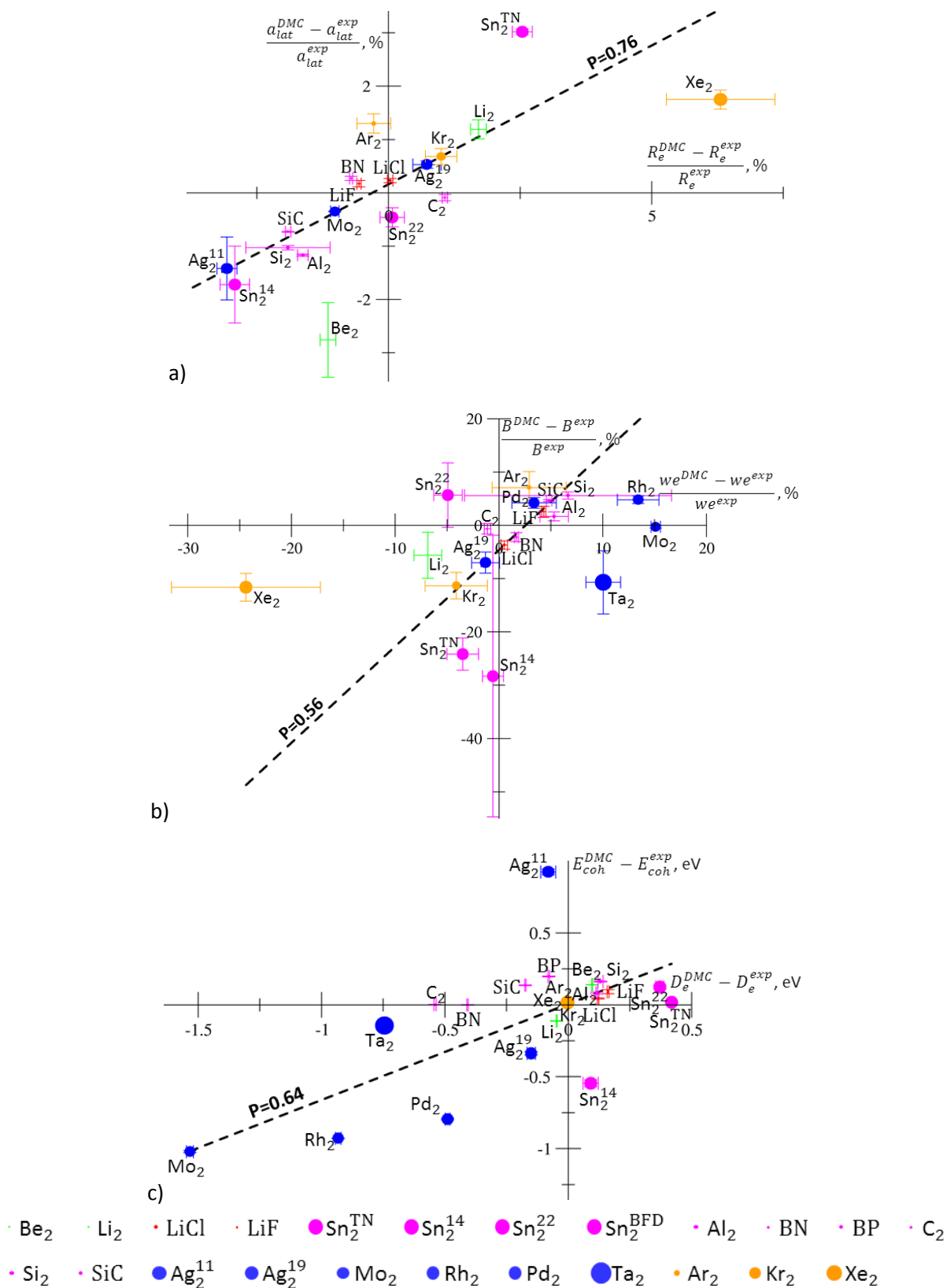


Fig. 6 Correlation between a) geometric, b) vibrational and c) energetic properties of solids and molecules from DMC calculations using the same pseudopotentials. Pearson correlation coefficient is shown above regression dashed lines.

There are additional effects, which are more difficult to include. Relativistic effects can impact the results especially for heavy elements. Despite the use of scalar relativistic pseudopotentials the DMC calculations has been performed without spin-orbit coupling. This can significantly affect the energetic properties - the cohesive energy of a solid or the dissociation energy of a molecule - because of the substantially different occupations of orbitals that occur for *j*-splitting compared to those without. We expect that the effect of spin-orbit coupling on the geometric and vibrational properties would be smaller by comparison [51]. Therefore, when comparing DMC results in solids and molecules one should rely more on the geometric and vibrational properties, noting that vibrational properties have larger statistical error bars compared to those associated with geometric properties.

There is a strong correlation between the deviation of DMC-computed geometric parameters from experiment in solids and molecules. Overestimation (underestimation) of optimal bond length is typically accompanied by an overestimation (underestimation) of the lattice parameter of solid (see Fig 6a). Molecules especially with d-d bonding and with p-p bonding show this correlation. The same type of correlation is seen for vibrational properties although the statistical error bars are larger (Fig. 6b). Despite strong spin-orbit coupling effects we can still see a correlation between energetics of solids and molecules (Fig. 6c). There is however a tendency to underestimate the dissociation energy for d-d molecules. This may be related to generally heavier elements selected in this group, which have larger relativistic effects and neutral atoms with high multiplicity. When relativistic effects are included the *j*-splitting of the partially filled orbitals of an atom can result in a lower energy compared to the non-relativistic non-split case, which can reduce the dissociation energy of a molecule. This is consistent with the large underestimation of dissociation energy we found for Mo<sub>2</sub>, which has 6 unpaired electrons in atom compared to all paired electrons in Mo<sub>2</sub> dimer.

We believe that the strong correlation we observe between the errors in calculated quantities for solids and molecules across a wide range of elements and pseudopotentials arises predominately from the errors due to the non-local pseudopotential even surpassing the effects of the fixed-node approximation, at least at the level of backflow. From a practical standpoint one can estimate the accuracy of DMC-computed properties of solids (and the accuracy of pseudopotentials) by first performing rather inexpensive calculations in molecules.

## Conclusion

We performed DMC calculations of the spectroscopic properties of molecules and of the equation of state parameters of solids. In addition, a careful analysis of the sources of our errors was made. One of the main reasons for disagreement between experiment and DMC results is the use of nonlocal pseudopotentials. While the use of pseudopotentials in any electronic structure approach invariably leads to approximations, including the neglect of core-core and core-valence correlation, the practical use of nonlocal of pseudopotentials in DMC requires the introduction of an additional approximation, the locality approximation. In this case DMC total energies depend on both the quality of the trial wave function in addition to its nodal structure. We showed how this approximation is not only large for systems containing heavier elements, but it also leads to additional complications during DMC calculations. In particular, DMC energies become very sensitive to the form of the trial wave function

and its degree of optimization. In practice, this means that accurate results are only obtained when both the variational freedom of the trial wave functions (e.g. Jastrows) as well as the level of optimization are carefully controlled. The mean-field nature of the nonlocal pseudopotential generation, using an approximate treatment of exchange and correlation which neglects important effects between the core and valence, combined with the locality approximation can potentially overwhelm the gains that arise from using such an accurate many-body method and yield incorrect descriptions of spectroscopic properties of molecules and EOS properties of solids. We show that the errors in molecules and solids are highly correlated. Thus a practical way to reduce the impact of including only an approximate treatment of the core-valence correlation is to first perform test calculations with the pseudopotential in similar molecular systems.

## Acknowledgements

Work by R.N., R.Q.H., and M.M. was performed under the auspices of the U.S. Department of Energy by Lawrence Livermore National Laboratory under Contract DE-AC52-07NA27344. This work has been supported by LDRD 13-ERD-067. L.S. was supported through the Predictive Theory and Modeling for Materials and Chemical Science program by the U.S. Department of Energy Office of Science, Basic Energy Sciences (BES). Sandia National Laboratories is a multiprogram laboratory operated by Sandia Corporation, a wholly owned subsidiary of Lockheed Martin Company, for the U. S. Department of Energy's National Nuclear Security Administration under Contract No. DE-AC04-94AL85000.

## References

- [1] M.J. Lucero, T.M. Henderson, and G.E. Scuseria, *J. Phys: Condens. Matter* **24**, 145504 (2012).
- [2] R. Nazarov, T. Hickel, and J. Neugebauer, *Phys. Rev. B* **85**, 144118 (2012).
- [3] A.E. Mattsson, R.R. Wixom, and R. Armiento, *Phys. Rev. B* **77**, 155211 (2008).
- [4] B. Grabowski, P. Söderlind, T. Hickel, and J. Neugebauer, *Phys. Rev. B* **84**, 214107 (2011).
- [5] K. Carling, G. Wahnström, T.R. Mattsson, A.E. Mattsson, N. Sandberg, and G. Grimvall, *Phys. Rev. Lett.* **85**, 3862 (2000).
- [6] D.M. Ceperley and B.J. Alder, *Phys. Rev. Lett.* **45**, 566 (1980).
- [7] C.J. Cramer, *Essentials of Computational Chemistry*. 2nd Edit. John Willey & Sons Ltd. (2004) England.
- [8] J. Cizek, *Adv. Chem. Phys.* **14**, 35 (1969).
- [9] P.J. Knowles and N.C. Handy, *Chem. Phys. Letters* **111**, 315 (1984).
- [10] G.H. Booth, A. Grüneis, G. Kresse, and A. Alavi, *Nature* **493**, 365 (2013).
- [11] W.M.C. Foulkes, L. Mitas, R.J. Needs, and G. Rajagopal, *Rev. Mod. Phys.* **73**, 33 (2001).
- [12] J. Kolorenc and L. Mitas, *Rep. Prog. Phys.* **74**, 026502 (2011).
- [13] G. Senatore and N. H. March, *Rev. Mod. Phys.* **66**, 445 (1994).
- [14] E. Gull, A.J. Millis, A.I. Lichtenstein, A.N. Rubtsov, M. Troyer, and P. Werner, *Rev. Mod. Phys.* **83**, 349 (2011).
- [15] S. Zhang and H. Krakauer, *Phys. Rev. Lett.* **90**, 136401 (2003).
- [16] D.M. Ceperley, *Rev. Mod. Phys.* **67**, 279 (1995).
- [17] S. Baroni and S. Moroni, *Phys. Rev. Lett.* **82**, 4745 (1999).
- [18] A.J. Williamson, R.Q. Hood, and J.C. Grossman, *Phys. Rev. Lett.* **87**, 246406 (2001).
- [19] M.J. Gillan, M.D. Towler, and D. Alfe, *Psi-k newsletter*, February (2011), [http://www.psi-k.org/newsletters/News\\_103/newsletter\\_103.pdf](http://www.psi-k.org/newsletters/News_103/newsletter_103.pdf)
- [20] K.P. Esler, J. Kim, D.M. Ceperley, and L. Shulenburger, *Computing in Science and Engineering*, **14**, 40 (2012).
- [21] Y. Kwon, D.M. Ceperley, and R.M. Martin, *Phys. Rev. B* **48**, 12037 (1993).
- [22] G. Ortiz, D.M. Ceperley, and R.M. Martin, *Phys. Rev. Lett.* **71**, 2777 (1993).
- [23] A. Ambrosetti, F. Pederiva, and E. Lipparini, *Phys. Rev. B* **83**, 155301 (2011).
- [24] C. Lin, F.H. Zong and D.M. Ceperley, *Phys. Rev. E* **64**, 016702 (2001).

- [25] R. Hood, P.R.C. Kent, and F.A. Reboredo, Phys. Rev. B **85**, 134109 (2012).
- [26] L.M. Fraser, W.M.C. Foulkes, G. Rajagopal, R.J. Needs, S.D. Kenny, and A.J. Williamson, Phys. Rev. B **53**, 1814 (1996).
- [27] A.J. Williamson, G. Rajagopal, R.J. Needs, L.M. Fraser, W.M.C. Foulkes, Y. Wang, and M.-Y. Chou, Phys. Rev. B **55**, 4851(R) (1997).
- [28] P.R.C. Kent, R.Q. Hood, A.J. Williamson, R.J. Needs, W.M.C. Foulkes, and G. Rajagopal, Phys. Rev. B **59**, 1917 (1999).
- [29] S. Chiesa, D.M. Ceperley, R. Martin, and M. Holzmann, Phys. Rev. Lett. **97**, 076404 (2006).
- [30] H. Kwee, S. Zhang, and H. Krakauer, Phys. Rev. Lett. **100**, 126404 (2008).
- [31] D.M. Ceperley, J. Stat. Phys. **43**, 816 (1986).
- [32] B. L. Hammond, P.J. Reynolds, and W.A. Lester Jr., J. Chem. Phys. **87**, 1130 (1987).
- [33] M. Dolg and X. Cao, Chem. Rev. **112**, 403 (2012).
- [34] W.C. Topp and J.J. Hopfield, Phys. Rev. B **7**, 1295 (1973).
- [35] J.C. Phillips, L. Kleinman, Phys. Rev. **116**, 287 (1959).
- [36] D.R. Hamann, M. Schlüter, and C. Chiang, Phys. Rev. Lett. **43**, 1494 (1979).
- [37] J.R. Trail and R.J. Needs, J. Chem. Phys. **122**, 014112 (2005).
- [38] J.R. Trail and R.J. Needs, J. Chem. Phys. **122**, 174109 (2005).
- [39] M. Burkatzki, C. Filippi and M. Dolg, J. Chem. Phys. **126**, 234105 (2007).
- [40] M. Burkatzki, C. Filippi and M. Dolg, J. Chem. Phys. **129**, 164115 (2008).
- [41] J.H. Wood and A.M. Boring, Phys. Rev. B **18**, 2701 (1978).
- [42] J.R. Trail and R.J. Needs, J. Chem. Phys. **139**, 014101 (2013).
- [43] J.R. Trail and R.J. Needs, J. Chem. Phys. **142**, 064110 (2015).
- [44] J.P. Perdew and A. Zunger, Phys. Rev. B **23**, 5048 (1981).
- [45] J.P. Perdew, K. Burke, and M. Ernzerhof, Phys. Rev. Lett. **77**, 3865 (1996).
- [46] J.P. Perdew, K. Burke, and M. Ernzerhof, Phys. Rev. Lett. **78**, 1396 (1997).
- [47] S. Fahy, X.W. Wang, and S.G. Louie, Phys. Rev. Lett. **61**, 1631 (1988).
- [48] S. Fahy, X.W. Wang, and S.G. Louie, Phys. Rev. B **42**, 3503 (1990).
- [49] S. Fahy, X.W. Wang, and S.G. Louie, Phys. Rev. B **43**, 9299 (1991).
- [50] L. Shulenburger and T. Mattsson, Phys. Rev. B **88**, 245117 (2013).
- [51] R. Hood, R. Nazarov, and M. Morales, in preparation.
- [52] R. Nazarov, R. Hood, M. Morales, in preparation.
- [53] C. Adamo and V. Barone, J. Chem. Phys. **110**, 6158 (1999).
- [54] J. Heyd, G. Scuseria, and M. Ernzerhof, J. Chem. Phys. **118**, 8207 (2003).
- [55] K. Kim and K.D. Jordan, J. Phys. Chem. **98**, 10089 (1994).
- [56] P.J. Stephens, F.J. Devlin, C.F. Chabalowski, and M.J. Frisch, J. Phys. Chem. **98**, 11623 (1994).
- [57] M. Dion, H. Rydberg, E. Schröder, D.C. Langreth, and B.I. Lundqvist, Phys. Rev. Lett. **92**, 246401 (2004).
- [58] C.W. Greef and J.W.A. Lester, J. Chem. Phys. **109**, 1607 (1998).
- [59] L. Shulenburger, T.R. Mattsson, M.P. Desjarlais, arXiv:1501.03850.
- [60] T.V. Russo, R.L. Martin, and P.J. Hay, J. Phys. Chem. **99**, 17085 (1995).
- [61] W.A. de Jong, R.J. Harrison, J.A. Nichols, D.A. Dixon, Theor. Chem. Acc. **107**, 22 (2001).
- [62] L. Mitáš, E.L. Shirley, and D. Ceperley, J. Chem. Phys. **95**, 3467 (1991).
- [63] N. Troullier and J.L. Martin, Phys. Rev. B **43**, 1993 (1991).
- [64] E.J. Walter, Opium Pseudopotential Generation Project, <http://opium.sourceforge.net>
- [65] I. Grinberg, N.J. Ramer, A.M. Rappe, Phys. Rev. B **62**, 2311 (2000).
- [66] F. Cygi, "Qbox: a large-scale parallel implementation of First-Principles Molecular Dynamics" (LLNL preprint, 2005).
- [67] L. Kleinman and D.M. Bylander, Phys. Rev. Lett. **48**, 1425 (1982).
- [68] P. Giannozzi, S. Baroni, N. Bonini, M. Calandra, R. Car, C. Cavazzoni, D. Ceresoli, G.L. Chiarotti, M. Cococcioni, I. Dabo, A. Dal Corso, S. de Gironcoli, S. Fabris, G. Fratesi, R. Gebauer, U. Gerstmann, C. Gougoussis, A. Kokalj, M. Lazzeri, L. Martin-Samos, N. Marzari, F. Mauri, R. Mazzarello, S. Paolini, A. Pasquarello, L. Paulatto, C. Sbraccia, S. Scandolo, G. Sclauzero, A.P. Seitsonen, A. Smogunov, P. Umari, and R.M. Wentzcovitch, J. Phys.:Condens.Matter, **21**, 395502 (2009).
- [69] M. Casula, Phys. Rev. B **74**, 161102 (2006).
- [70] N.D. Drummond, M.D. Towler, and R.J. Needs, Phys. Rev. B **70**, 235119 (2004).
- [71] N.D. Drummond and R.J. Needs, Phys. Rev. B **72**, 085124 (2005).

- [72] R. J. Needs, M. D. Towler, N. D. Drummond, and P. López Ríos, *J. Phys. Condens. Matter* **22**, 023201 (2010).
- [73] J. Kim, K.P. Esler, J. McMinis, M. Morales, B.K. Clark, L. Shulenburger, and D. Ceperley, *J. Phys: Conference Series*. **402**, 012008 (2012).
- [74] D. Alfe and M.J. Gillan, *Phys. Rev. B* **70**, 161101 (2004).
- [75] N. D. Drummond, R. J. Needs, A. Sorouri, and W. M. C. Foulkes, *Phys. Rev. B* **78**, 125106 (2008).
- [76] P.M. Morse, *Phys. Rev.* **34** (1929) 57.
- [77] F.D. Murnaghan, *Proc. N.A.S.* **30**, 244 (1944).
- [78] P. Vinet, J. Ferrante, J.R. Smith, and J.H. Rose, *J. Phys. C: Solid State Phys.* **19**, L467 (1986).
- [79] B. Efron and R. Tibshirani, *An Introduction to the Bootstrap*. (Boca Raton, FL: Chapman & Hall/CRC, 1993).
- [80] B. Simard, P.A. Hackett, A.M. James, P.R.R. Langridge-Smith, *Chem. Phys. Lett.* **186**, 415 (1991).
- [81] R.O. Jones, *J. Chem. Phys.* **99**, 1194 (1993).
- [82] J.F. Ogilvie and F.Y.H. Wang, *J. Mol. Struct.* **273**, 277 (1992).
- [83] NIST Computational Chemistry Comparison and Benchmark Database, NIST Standard Reference Database Number 101, Release 16a, August 2013, Editor: Russell D. Johnson, <http://cccbdb.nist.gov/>
- [84] Yu.M. Efremov, A.N. Samoilova, V.B. Kozhukhovskiy, and L.V. Gurvich, *J. Mol. Spectr.* **73**, 430 (1978).
- [85] R.R. Reddy, T.V.R. Rao, R. Viswanath, *Astrophys. Space Science* **189**, 29 (1992).
- [86] K. Pak, M.F. Cai, T.P. Dzuga and V.E. Bondybey, *Faraday Discuss. Chem. Soc.* **86**, 153 (1988).
- [87] *Handbook of Chemistry and Physics* (2015) [www.hbcponline.com](http://www.hbcponline.com).
- [88] B. Simard, M.-A. Lebeault-Dorget, A. Marijnissen, and J.J. ter Meulen, *J. Chem. Phys.* **108**, 9668 (1998).
- [89] I. Shim and K. Gingerich, *J. Chem. Phys.* **80**, 5107 (1984).
- [90] D.L. Cocke and K.A. Gingerich, *J. Chem. Phys.* **60**, 1958 (1974).
- [91] V.I. Srdanov and D.S. Pesic, *J. Mol. Spectr.* **90**, 27 (1981).
- [92] S.S. Lin, B. Strauss and A. Kant, *J. Chem. Phys.* **51**, 2282 (1969).
- [93] H. Wang, H. Haouari, R. Craig, Y. Liu, J.R. Lombardi, and D.M. Lindsay, *J. Chem. Phys.* **106**, 2101 (1997).
- [94] K. Balasubramanian and K. Pitzer, *J. Chem. Phys.* **78**, 321 (1983).
- [95] Z. Hu, B. Shen, J.R. Lombardi, and D.M. Lindsay, *J. Chem. Phys.* **96**, 8758 (1992).
- [96] K. Lejaeghere, V. Van Speybroeck, G. Van Oost, and S. Cottenier, *Crit. Rev. in Solid State and Mater. Sci.* **39**, 1 (2014).
- [97] C. Kittel, *Introduction to Solid State Physics*, 8th ed. (John Wiley & Sons, Inc, 2005).
- [98] P. Villars and J. Daams, *J. Alloys Compd.* **197**, 177 (1993).
- [99] C.J. Buchenauer and J.M. Rowe, *Solid State Commun.* **7**, 1433 (1969).
- [100] K. Foyevtsiva, J.T. Krogel, J. Kim, P.R.C. Kent, E. Dagotto, and F.A. Reboredo, *Phys. Rev. X* **4**, 031003 (2014).
- [101] P. López Ríos, A. Man, N.D. Drummond, M.D. Towler, and R.J. Needs, *Phys. Rev. E* **74**, 066701 (2006).